Biomechanical Analysis of Volar and Dorsal Double Locking Plates for Fixation in Comminuted Extra-articular Distal Radius Fractures: A 3D Finite Element Study

Yu-Hao Lin[1,†] Chun-Li Lin[2,†] Hsien-Nan Kuo[3] Ming-Tsung Sun[1]

Alvin Chao-Yu Chen[4,*]

[1]*Department of Mechanical Engineering, Chang Gung University, Taoyuan 333, Taiwan, ROC*
[2]*Department of Biomedical Engineering, National Yang-Ming University, Taipei 112, Taiwan, ROC*
[3]*Medical Devices Development Section, Metal Industries Research & Development Centre, Kaohsiung 821, Taiwan, ROC*
[4]*Department of Orthopaedic Surgery, Chang Gung Memorial Hospital, Taoyuan 333, Taiwan, ROC*

Received 28 Aug 2011; Accepted 14 Nov 2011; doi: 10.5405/jmbe.1003

Abstract

The effects of fracture type, fixation approach, and postoperative functional load factors on the biomechanical interactions in extra-articular distal radius fractures are investigated using three-dimensional (3D) finite element (FE) analysis. 3D distal radius fracture FE models with dorsal wedge, metaphyseal, and volar wedge fractures and volar plating (VP) and dorsal double plating (DDP), respectively, are constructed based on computed tomography images. After model verification and validation, the interface between the fixation plates and the bony surface is simulated using frictional (contact) elements. The von Mises stress distribution and displacements at the radius end are observed under axial, bending, and torsion load conditions. The simulation results indicate that the stress in the bone and fixation plates is higher under bending and torsion loading than under axial loading. The stress values for the bone and fixation plates with DDP fixation are generally lower than those obtained with VP fixation (bone stress is around 31-53% lower and plate stress is around 75% lower). The total displacements of the fracture site with DDP fixation are on average 87.5% lower than those obtained with VP fixation. Postoperative bending and torsion loads should be avoided as much as possible to decrease the stress on the bone and fixation plates. DDP fixation provides better mechanical strength compared to that of VP fixation, decreasing the risk of displacement and stress concentration for distal extra-articular radius fractures.

Keywords: Biomechanics, Distal radius fracture, Dorsal double plating, Volar plating, Finite element analysis

1. Introduction

Fractures in the distal radius region are among the most common skeletal injuries. Treatment objectives are to gain and maintain anatomical reduction while the fracture heals, restore painless wrist motion and strength, and avoid typical complications [1-3]. Rigid internal fixation has become a common method of treatment for many unstable articular or periarticular fractures [3,4].

Traditionally, plate fixation for dorsally comminuted distal radius fractures has been performed with dorsal placement. However, such placement is associated with extensor tendon irritation, attrition, and frank rupture complications [3,5,6]. Volar plating (VP) of dorsally displaced fractures with conventional plates has been shown to give good clinical results in younger patients and with fractures of various complexities [7,8]. However, a volar plate has no buttress effect in dorsally comminuted and displaced fractures and might have insufficient strength in elderly osteoporotic patients [9]. Dorsal plating constructs with a lower profile have been made to minimize soft-tissue complications, and have achieved improved clinical success [10]. The dorsal double plating (DDP) technique based on the three-column distal radius and ulna concept can reestablish radio-ulnar congruency to achieve early stability and function and has demonstrated clinical success [1,4,11].

Plates with locking screws that have greater stiffness and strength than those of standard plates have been developed to reduce the possibility of screw loosening and subsequent loss

† These authors contributed equally to this work
* Corresponding author: Alvin Chao-Yu Chen
Tel: +886-3-3281200 ext. 3882; Fax: +886-3-3284564
E-mail: ymbmecaeb@gmail.com

of reduction. These locking plates may also allow for increased periosteal blood supply and eliminate the need for extreme contouring to match the shape of the radius [12,13]. Therefore, modalities of internal fixation for the distal radius have been developed to allow the screws to be locked into the plate, which ensures axial as well as angular stability for both VP or low-profile DDP approaches.

Distal radius fractures are classified into nine kinds of fracture by the administrative officer (AO) foundation. Selection of the most appropriate therapy depends on the configuration and sort of fracture [14-16]. Biomechanical aspects, such as distal bone segment displacement and bone/plate/screw stress in various configurations are usually major factors for evaluating the fixation system treatment success rate. However, there is ideal fixation for the distal radius and optimal treatment remains a therapeutic challenge [3,17,18].

Although clinical studies are the ultimate investigative tool, it is often difficult to identify and isolate important parameters due to confounding variables. Cadaver studies are limited by the problems created when performing several comparative experiments on a given specimen. The finite element (FE) method provides mechanical responses and allows parameters to be adjusted in a more controllable manner, and is thus commonly used as an analytical tool in biomechanical studies [19,20]. The present study evaluates the effects of fracture type (dorsal wedge, metaphyseal, and volar wedge fractures), fixation type (VP and DDP fixations), and immediate postoperative functional load (axial, bending, and torsion loadings) on biomechanical responses using three-dimensional (3D) FE analysis.

2. Materials and methods

The fracture type, internal fixation type, and immediate postoperative functional load were considered. The fracture pattern was assumed to be one of three types, namely dorsal wedge, metaphyseal, and volar wedge fractures, according to the 23-A2 classification of the AO Surgery Reference (Fig. 1-a) [5]. These fracture types are simple extra-articular fractures with a dorsal tilt (Colles fractures) (Fig. 1-a1), undisplaced fractures with impaction but no abnormal palmar or dorsal tilt (Fig. 1-a2), and simple extra-articular fractures with impaction and volar tilt (Goyrand-Smith fractures) (Fig. 1-a3), respectively.

Two low-profile titanium VP and DDP locking plates with 2.4 mm screws were used for all fracture types to evaluate the corresponding biomechanical responses. A pre-contoured plate system (Synthes Ltd., Paoli, PA, USA) that offers volar, dorsal, and styloid fixation options with locking head screws, forming an angle-stable construct, was used. The VP was shaped to the articular curve and placed on the osteotomy surface (Fig. 1-b2). DDPs were designated for placement on the dorso-ulnar side for the intermediate plate (between the second and third compartments) and the dorso-radial side for the styloid plate (underneath the second extensor compartment) (Fig. 1-b1). All plates were implanted according to the manufactures' guidelines and were of similar length.

The geometry and anatomical relationship of the left radius were reconstructed from computed tomography (CT) images of an intact healthy male. Images were taken using 80 scans at intervals of 1 mm in the transverse plane direction. The digitalized images were input into image processing software Amira 4.1 (Mercury Computer Systems, Germany) for reconstruction. The inner and outer cortical bone contours were extracted and converted into mathematical entities. The parallel contours of the inner/outer cortical bone contours were then input into an FE package (ANSYS, Version 11.0, Swanson Analysis Inc., Houston, TX, USA) to generate solid cancellous and cortical bone models. A 3-mm gap, a 35-degree wedge toward the dorsal and volar sites, 25 mm from the distal end of the radius, was created using an idealized planar cut to simulate the three fracture types (Fig. 1-a). Solid models of the plates and screws were generated in a CAD system (Pro/Engineering, Parametric Technology Co., MA, USA) and imported into ANSYS to assemble the bone/plate fixation system (Fig. 1-b). The locking screw thread details were excluded because the mechanical response at the thread/bone interface was not the focus of this study.

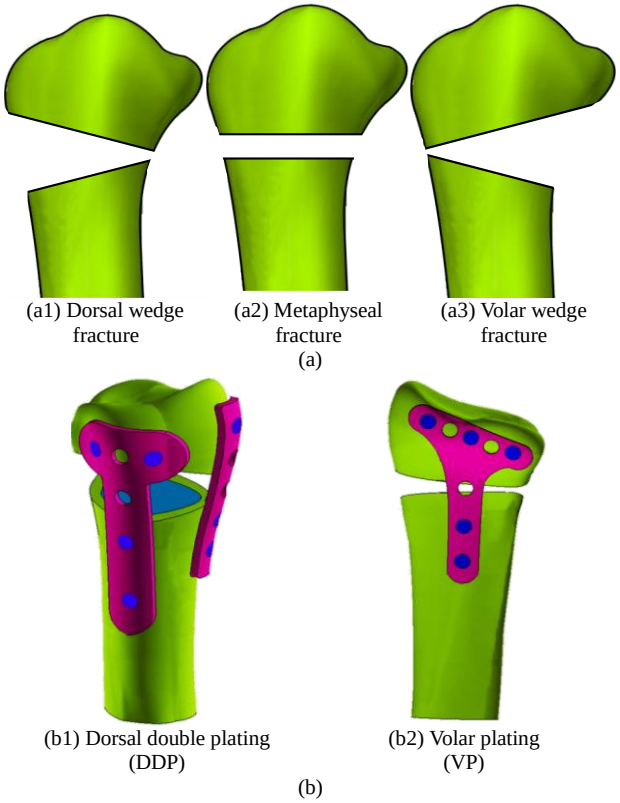

Figure 1. (a) Solid model construction of the distal radius with (a1) dorsal wedge fracture, (a2) metaphyseal fracture, and (a3) volar wedge fracture. (b) Solid model construction of the distal radius with (b1) dorsal double plating and (b2) volar plating.

A convergence test was used to guarantee that the numerical model reached the converged results (difference of each model within 5%) and that no further mesh refinement

was necessary. Single mesh patterns of the intact radius FE models with 1-, 2-, and 3-mm smart (automatic creating reasonably shaped elements) element sizes (edge lengths) were generated on unitary solid model using quadratic tetrahedral elements (Solid 92) in ANSYS. The cortical and cancellous bones were assumed to be linear, elastic, and isotropic, with elastic modulii of 17 GPa and 1.3 GPa, respectively. Poisson's ratio was taken as 0.3 [20]. The models were constrained at the proximal end with an axial load of 100 N applied at the center of the articular surface. The convergence criteria were based on the total strain energy and displacement values at the fracture gap. The tolerance level was set as a change of less than 5%.

The FE model was validated by comparing the predicted values to Gesensway et al.'s cadaver study results [21]. In their experiment, the T plate was designed to buttress simple partial articular fractures of the distal radius. The rigidity (defined as the slope of the straight-line region of the load- displacement curve) was recorded to represent the strength of the T plate in five fresh-cadaver compressive tests with the extra-articular radius fracture type. To simulate this setting, the VP model was constrained at the proximal end with axial compressive loads of 10, 25, 50, and 100 N applied at the center of the articular surface. The elastic modulus and Poisson's ratio of the titanium plates/screws were 110 GPa and 0.3, respectively [20,22]. The rigidities of the load conditions were calculated from the corresponding axial load- displacement curves.

The resulting FE model was meshed using a 1-mm smart element size after the convergence test (Figs. 2b and 2c). To simulate a more realistic interfacial condition, the locking screws were assumed to have continuous connections with the fixation plates, and cortical and cancellous bones. The bonded condition was used to mimic the screw/plate and screw/bone interfaces. Nonlinear contact elements (defined as surface to surface) with friction coefficients of 0.3 were used to simulate the interfacial adaptation between the fixation plates and bony surface [20]. An axial load of 100 N and bending and torsion moment loads of 1 Nm were applied at the end of the distal radius under the boundary condition and material properties used in the convergence test (Fig. 2a) [23-26]. The magnitudes and directions of the applied loads simulated the physiological loads experienced with active wrist joint movement during daily activities [23,25,27]. Eighteen FE models with three fracture types, two fixation types, and three load conditions, respectively, were simulated in this study. To investigate the wrist load transmission pattern and check the potential for fracture fragment loosening, the displacements at the fracture gap of the distal radius (average in all directions) and the von Mises stresses of the radius bone and fixation plates were recorded.

3. Results

The numbers of nodes and elements for the three mesh models in the convergence test are listed in Table 1. Differences in the strain energies of the models and displacements in the radius end were within 5%, showing that numerical convergence was achieved. The resulting FE model was meshed using a 1-mm smart element size for further analyses to avoid geometry distortion. For the radius FE model validation, the rigidity was 1.57 ± 0.51 N/mm (mean ± standard deviation) in Gesensway et al.'s study and 1.49 N/mm in the present study. The percentage error compared with the experimental result was 5.1%, which indicates that the radius FE model was reasonable.

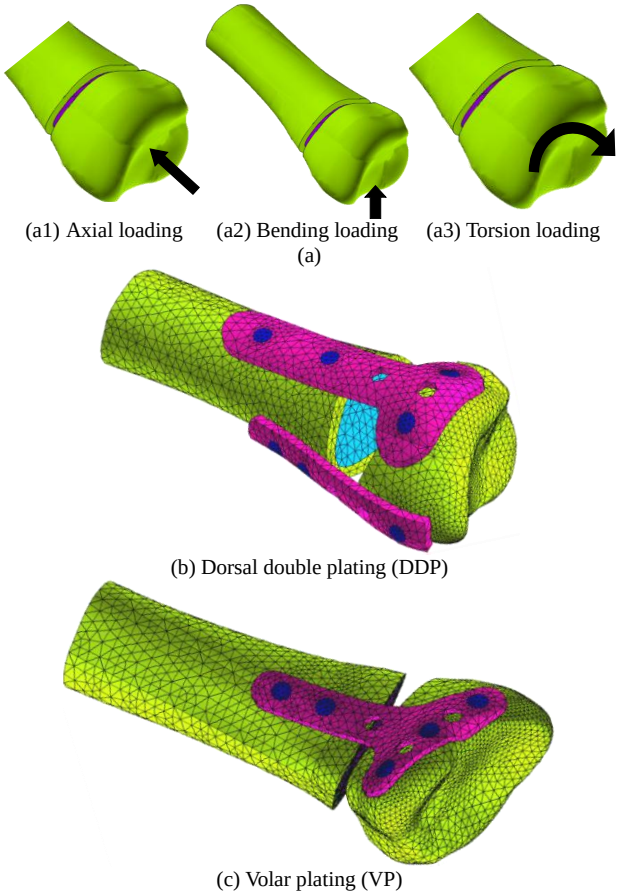

Figure 2. FE mesh model with two fixation types and three load conditions. (a) Load contitions: (a1) axial loading, (a2) bending loading, and (a3) torsion loading. 3D FE model with (b) DDP and (c) VP.

Table 1. Numbers of nodes and elements, strain energy, displacement at the radius end, and von Mises stress at the fracture gap of the three mesh models in the convergence test.

Element Size (mm)	Number of elements	Number of nodes	Strain energy (J)	Error (%)	Displacement at radius end (mm)	Error* (%)
3.0	100967	125589	3.28484	3.38	0.11913	0.06
2.0	105609	133223	3.40207	1.11	0.11916	0.03
1.0	121675	181117	3.44011	0	0.1192	0

*Error (%) = strain energy (smart size 1.0) - strain energy (smart size 3.0/2.0)*100% / strain energy (smart size 1.0)

Figure 3 shows the maximum von Mises stress for bone (σBone_max) for various fracture types and VP/DDP fixations under axial, bending, and torsion loads. In general, the bending and torsion conditions give significantly higher σBone_max values compared to that obtained under axial loading. The σBone_max values for DDP fixation were in general lower than those for the VP fixation. The percentage error for the value was around 31%-53%. No obvious differences in stress values

were found for the fracture types under the given VP/DDP fixations and axial/bending/torsion loads. Figure 4 shows the maximum von Mises stress for a fixation plate (σPlate_max) for various fracture types and VP/DDP fixations under axial, bending, and torsion loads. DDP fixation produced 75% lower stress (σPlate_max) than the values for VP fixation.

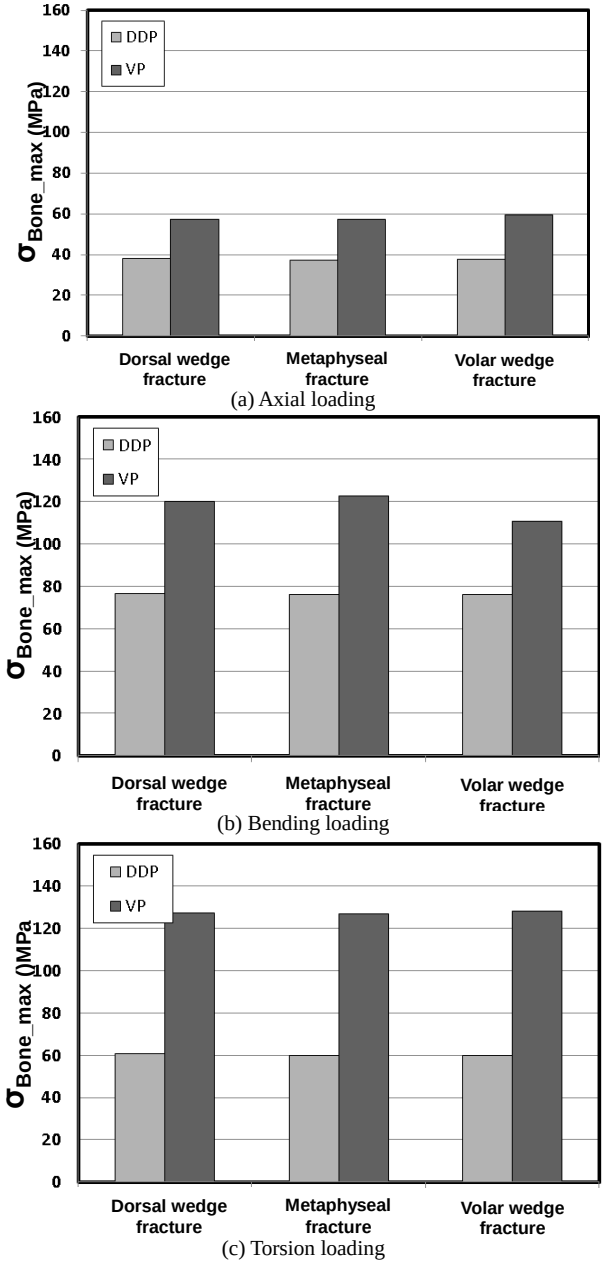

Figure 3. Maximum von Mises stress values in distal radius (σBone_max) for with two fixation types under (a) axial, (b) bending, and (c) torsion loads.

The stress distributions for all models under a given fracture type were similar. Figures 5 and 6 show the bone and plate von Mises stress distributions with VP/DDP fixation under axial/bending/torsion loads for the metaphyseal fracture. Figure 5 shows that the σBone_max values were obtained around the screw hole and that the locations depend on the load conditions. The σBone_max value was near the fractured gap

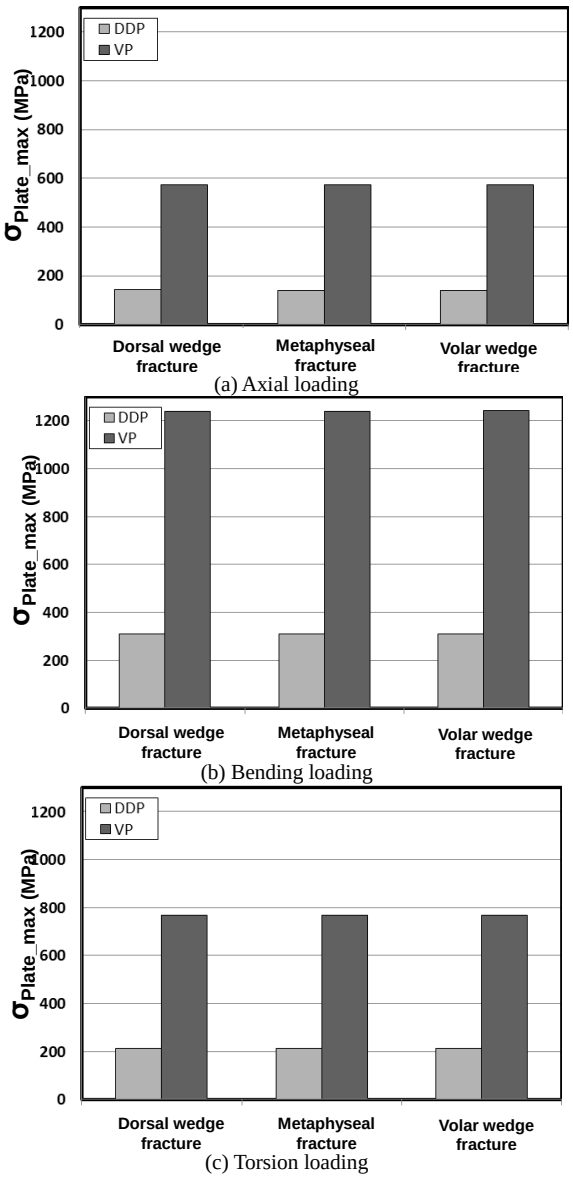

Figure 4. Maximum von Mises stress values in fixation plate (σPlate_max) with two fixation types under (a) axial, (b) bending, and (c) torsion loads.

under axial loading and around the proximal first screw under bending and torsion conditions. Figure 6 shows the σPlate_max values for the metaphyseal fracture under axial/bending/torsion conditions. The stress was concentrated near the fracture gap for DDP fixation and around the proximal first screw for VP fixation.

The total fracture site displacements for all models were recorded to observe the early motion after the operation. Results are shown in Fig. 7. The displacements for DDP fixation were on average 87.5% lower than those for VP fixation. Regardless of the fixation type, the displacement was highest under bending, followed by torsion and axial loads. With VP fixation, the displacements for the dorsal/volar wedge fractures were slightly higher than that for the metaphyseal fracture under bending and torsion conditions.

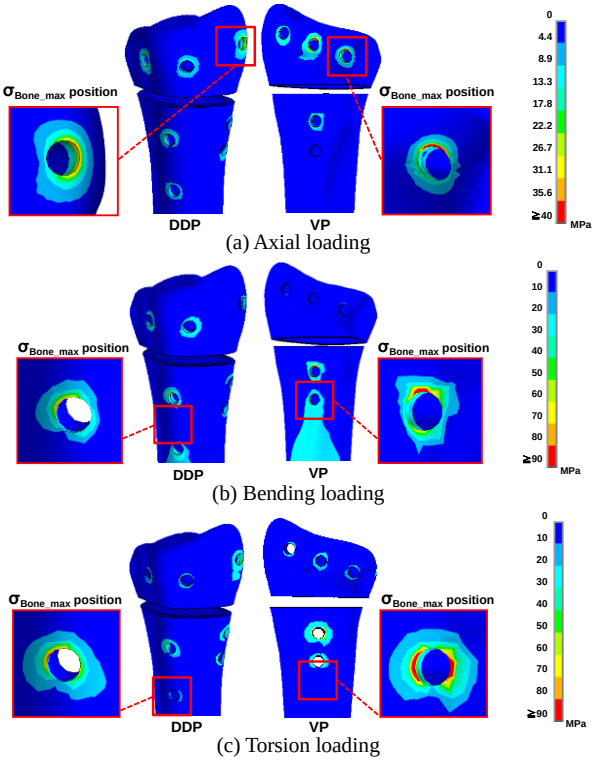

Figure 5. Stress distributions and σBone_max positions of the models with metaphyseal fracture and two fixation types under (a) axial, (b) bending, and (c) torsion loads.

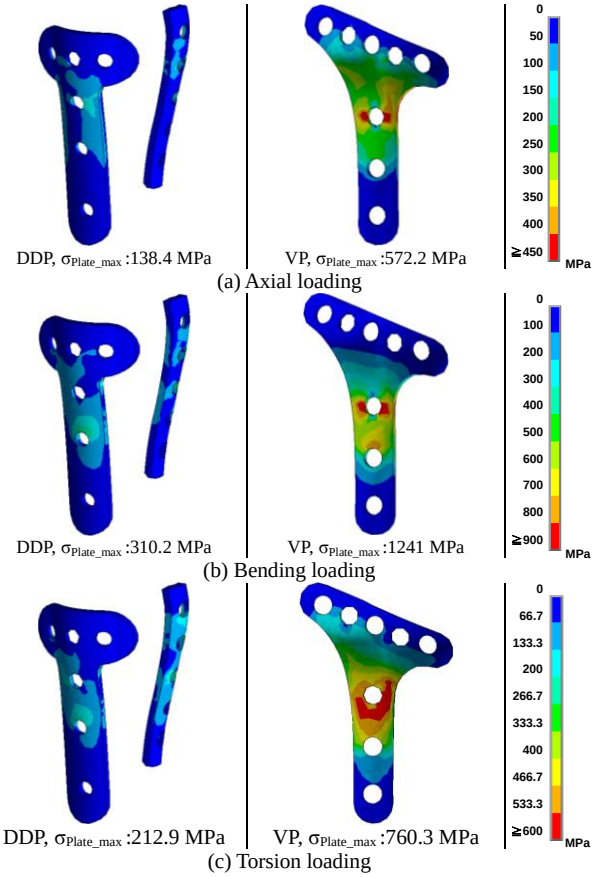

Figure 6. Stress distributions and σPlate_max values of the models with metaphyseal fracture and two fixation types under (a) axial, (b) bending, and (c) torsion loads.

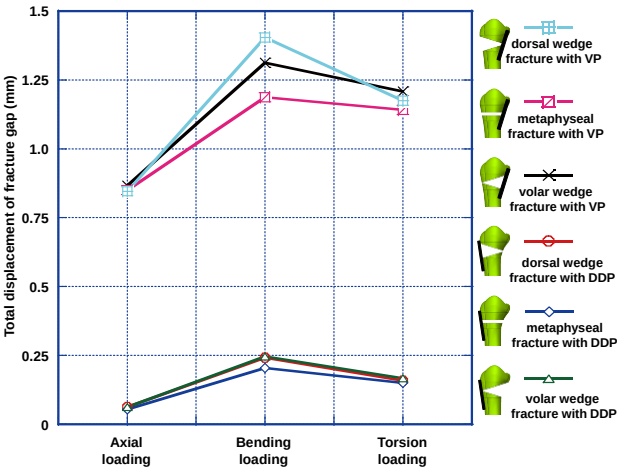

Figure 7. Displacements at the radius gap for all simulated models.

4. Discussion

Distal radial fractures are often seen in the elderly and the very young. There is increased enthusiasm for operative treatment of distal radius fractures [14-16]. Numerous internal fixation techniques are implemented by surgeons. An optimum technique should not only restore wrist alignment but also restore joint function.

Sometimes the dorsal fracture exhibits more trends to the comminuted configurations. When there is insufficient space for dorsal fixation, volar fixation is a reasonable alternative. This study compared the stability of VP and DPP constructs in a simulated comminuted extra-articular distal radius fracture. Both constructs withstood postoperative functional loads. The simulation results indicate that the fixation type and load conditions affect the stress value/distribution and the displacement at the fracture gap in a radial fracture fixation system. Bending and torsion loads produce a higher moment force on the bone and fixation plates, and thus significantly higher stress values, compared to that produced by axial loading, regardless of the fixation type [18]. For the dorsal and styloid construct (DDP fixation), the two plates placed on different columns and the cross structure provide better strength against wrist loads than the single VP. The dorsal plates buttressed and bridged the defect on the dorsum of the radius while the volar cortex was in contact. Failure occurred because of slippage or fracture in the volar cortex. This is in agreement with the findings of a previous biomechanical study [5,9]. Although an opening volar wedge osteotomy for mal-union also has a loss of volar bony support, VP fixation has no particular biomechanical advantage in extra-articular fractures. The results also reveal that there are no significant differences in stress and displacement values among the fracture types.

Problems such as screw loosening, plate fracture, and misalignment might occur with high stress concentrated on the bone and plate. The stress concentration locations for the plate were near the fracture gap for axial loading, under which a compressive force is induced in these areas. The corresponding locations for bending and torsion conditions are at the first hole near the fracture gap at the proximal site were the branch points by virtue of these areas. The osteotomy gap was positioned

over this hole in all constructs. It was not filled with a screw and the stress was concentrated in this area of the plate. The elongated hole may represent a region of weakness due to the decreased plate cross-sectional area and may warrant reinforcement. DDP divides the stress between the two plates, and can thus resist a higher moment than VP, reducing the risk of screw loosening and plate fracture.

Clinically, a larger displacement can cause dislocation and create an unstable structure. Fracture fragment displacement is an important factor governing whether the fracture will heal and the mechanism through which the bone unites, such as periosteal or endosteal union. The tendency of the average displacements at the fracture gap is similar to that of the stress value/distribution. The displacement with DDP fixation was much lower than that with VP fixation, indicating that the former has better structural strength.

Nonlinear FE analysis is a complementary tool for reflecting the feasibility, efficacy and to quantify the fixation type mechanical responses. The radius model was generated from intact healthy male CT data. The thickness of the cortex bone in the model, measured directly from the CT image data, was 1.0-1.2 mm at the dorsal site and 1.5-1.9 mm at the volar site 10 mm away from the articular surface. These thickness values are similar to those reported by Dhillon, who compared the thickness of the volar and dorsal cortices of cadaveric adult radii using digital photography and found that the thickness of the cortex bone was 0.71 ± 0.22 mm at the dorsal site and 1.49 ± 0.33 mm at volar site [28]. However, there were some limitations in the present study, including assumptions of bone material properties, screw geometry, and load conditions, which may affect the accuracy of the results. Linear elastic (homogeneous and isotropic) characterization of the bone and plate/screw were used to simplify the numerical convergence considerations. A bonded interface was used to mimic the interface fixation between the screw and bone considering that the screw provides appropriate connection and the stress is continuously transmitted from screw to bone. The global stress values on the bone, screw, and plate are not affected by local mechanical responses on the thread/bone interface based on Saint-Venant's principle [29]. Consequently, frictional contact conditions were employed only at the interface between the plate and bony surface. The three load types used in this study did not simulate realistic tendon forces on specific activation muscles. Only the potentials for axial, bending, and torsion forces were determined in the wrist joint. The magnitudes of the applied 100-N and 1-Nm loads were comparable to the physiological loads expected with active wrist joint motion and loads across the wrist joint during daily living activities [23-26]. Therefore, the modeling results merely provide a general insight into the mechanical and biomechanical aspects and suggestions for clinical treatment.

5. Conclusion

Biomechanical analysis results reveal that the fixation type and load conditions affect the stress value/distribution and fracture fragment displacement for various distal extra-articular radius fractures. Bending and torsion create significantly higher stress values than those obtained under axial loading. DDP fixation provides better mechanical strength to prevent displacement and establishes better stress transmission than those of VP fixation for distal radius fractures.

References

[1] R. Peine R, D. A. Rikli, R. Hoffmann, G. Duda and P. Regazzoni, "Comparison of three different plating techniques for the dorsum of the distal radius: a biomechanical study," J. Hand Surg. Am., 25: 29-33, 2000.

[2] J. B. Jupiter and H. Lipton, "The operative treatment of intraarticular fractures of the distal radius," Clin. Orthop. Relat. Res., 292: 48-61, 1993.

[3] D. A. Rikli and P. Regazzoni, "Fractures of the distal end of the radius treated by internal fixation and early function. A preliminary report of 20 cases," J. Bone Joint Surg. Br., 78: 588-592, 1996.

[4] M. Jakob, D. A. Rikli and P. Regazzoni, "Fracture of the distal radius treated by internal fixation and early function," J. Bone Joint Surg. Br., 82: 340-344, 2000.

[5] C. Trease, T. McIff and E. B. Toby, "Locking versus nonlocking t-plates for dorsal and volar fixation of dorsally comminuted distal radius fractures: a biomechanical study," J. Hand Surg. Am., 30: 756-763, 2005.

[6] G. K. Kambouroglou and T. S. Axelrod, "Complications of the AO/ASIF titanium distal radius plate system (pi plate) in internal fixation of the distal radius: a brief report," J. Hand Surg. Am., 23: 737-741, 1998.

[7] M. Kamano, Y. Honda, K. Kazuki and M. Yasuda, "Palmar plating for dorsally displaced fractures of the distal radius," Clin. Orthop. Rel. Res., 397: 403-408, 2002.

[8] K. J. Constantine, M. C. Clawson and P. J. Stern, "Volar neutralization plate fixation of dorsally displaced distal radius fractures," Orthopedics, 25: 125-128, 2002.

[9] M. Blythe, K. Stoffel, P. Jarrett and M. Kuster, "Volar versus dorsal locking plates with and without radial styloid locking plates for the fixation of dorsally comminuted distal radius fractures: a biomechanical study in cadavers," J. Hand Surg. Am. 31: 1587-1593, 2006.

[10] A. F. Kamath, D. Zurakowski and C. S. Day, "Low-profile dorsal plating for dorsally angulated distal radius fractures: an outcomes study," J. Hand Surg. Am., 31: 1061-1067, 2006.

[11] D. A. Rikli, R. Curtis, C. Schilling and J. Goldhahn, "The potential of bioresorbable plates and screws in distal radius fracture fixation," Injury, 33: B77-B83, 2002.

[12] S. M. Perren, "Evolution and rationale of locked internal fixator technology. Introductory remarks," Injury, 32 Suppl. 2: B3-B9, 2001.

[13] M. Florin, M. Arzdorf, B. Linke and J. A. Auer, "Assessment of stiffness and strength of 4 different implants available for equine fracture treatment: a study on a 20 degrees oblique long-bone fracture model using a bone substitute," Vet. Surg., 34: 231-238, 2005.

[14] S. Graff and J. B. Jupiter, "Fracture of the distal radius: classification of treatment and indications for external fixation," Injury, 25 Suppl 4: SD14-SD25, 1994.

[15] R. D. Renee, B. D. Adams and V. K. Goel, "An analysis of bone stresses and fixation stability using a finite element model of simulated distal radius fractures," J. Hand Surg. Am., 27: 86-92, 2002.

[16] W. H. Short, A. K. Palmer, F. W. Werner and D. J. Murphy, "A biomechanical study of distal radial fracture," J. Hand Surg. Am., 12: 529-534, 1987.

[17] P. W. Howard, H. D. Stewart, R. E. Hind and F. D. Burke, "External fixation or plaster for severely displaced comminuted Colles' fractures? A prospective study of anatomical and functional results," J. Bone Joint Surg. Br., 71: 68-73, 1989.

[18] J. B. Jupiter, "Complex articular fractures of the distal radius: classification and management," J. Am. Acad. Orthop. Surg., 5: 119-129, 1997.

[19] C. L. Lin, J. C. Wang and Y. C. Kuo, "Numerical simulation on the biomechanical interactions of tooth/implant-supported system under various occlusal forces with rigid/non-rigid connections," J. Biomech., 39: 453-463, 2006.
[20] C. J. Brown, C. J. Wang, A. L. Yettram and P. Procter, "Intramedullary nails with two lag screws," Clin. Biomech., 19: 519-525, 2004.
[21] D. Gesensway, M. D. Putnam, P. L. Mente and J. L. Lewis, "Design and biomechanics of a plate for the distal radius," J. Hand Surg. Am., 20: 1021-1027, 1995.
[22] C. F. Scifert, T. D. Brown and J. D. Lipman, "Finite element analysis of a novel design approach to resisting total hip dislocation," Clin. Biomech., 14: 697-703, 1999.
[23] K. N. An, E. Y. Chao, W. P. Cooney and R. L. Linscheid, "Forces in the normal and abnormal hand," J. Orthop. Res., 3: 202-211, 1985.
[24] W. P. Cooney 3rd and E. Y. Chao, "Biomechanical analysis of static forces in the thumb during hand function," J. Bone Joint Surg. Am., 59: 27-36, 1977.
[25] M. D. Putnam, N. J. Meyer, E. W. Nelson, D. Gesensway and J. L. Lewis, "Distal radial metaphyseal forces in the extrinsic grip model: implications for postfracture rehabilitation," J. Hand Surg. Am., 25: 469-475, 2000.
[26] S. W. Wolfe, C. R. Swigart, J. Grauer, J. F. Slade and M. M. Panjabi, "Augmented external fixation of distal radius fractures: a biomechanical analysis," J. Hand Surg. Am., 23: 127-134, 1998.
[27] D. Osada, S. Fujita, K. Tamai, A. Iwamoto, K. Tomizawa and K. Saotome, "Biomechanics in uniaxial compression of three distal radius volar plates," J. Hand Surg. Am., 29: 446-451, 2004.
[28] S. S. Dhillon, A. J. Kumar, V. Sadaiyyappan, R. S. Bassi, D. Shanahan and S. C. Deshmukh, "Anatomical study comparing the thickness of the volar and dorsal cortex of cadaveric adult distal radii using digital photography," Arch. Orthop. Trauma Surg., 127: 975-977, 2007.
[29] Y. C. Fang, "A first course in continuum mechanics, 2nd edn," NJ: Prentice-Hall Inc., 1977.